Excess ''read-through'' acetylcholinesterase attenuates but the ''synaptic'' variant intensifies neurodeterioration correlates

Meira Sternfeld*†, Shai Shoham‡, Omer Klein*, Cesar Flores-Flores*, Tamah Evron*, Gregory H. Idelson§, Dani Kitsberg§, James W. Patrick¶, and Hermona Soreq*‖

*The Eric Roland Center for Neurodegenerative Diseases, Department of Biological Chemistry, Hebrew University of Jerusalem, Jerusalem 91904, Israel; ‡Research Department, Herzog Hospital, Jerusalem 91351, Israel; §Alomone Labs, P.O. Box 4287, Jerusalem 91042, Israel; and ¶Baylor College of Medicine, Division of Neuroscience, One Baylor Plaza, Houston, TX 77030-3498

Edited by Tomas Hökfelt, Karolinska Institute, Stockholm, Sweden, and approved May 10, 2000 (received for review January 6, 2000)

Acute stress increases the risk for neurodegeneration, but the molecular signals regulating the shift from transient stress responses to progressive disease are not yet known. The ''read-through'' variant of acetylcholinesterase (AChE-R) accumulates in the mammalian brain under acute stress. Therefore, markers of neurodeterioration were examined in transgenic mice overexpressing either AChE-R or the ''synaptic'' AChE variant, AChE-S. Several observations demonstrate that excess AChE-R attenuates, whereas AChE-S intensifies, neurodeterioration. In the somatosensory cortex, AChE-S transgenics, but not AChE-R or control FVB/N mice, displayed a high density of curled neuronal processes indicative of hyperexcitation. In the hippocampus, AChE-S and control mice, but not AChE-R transgenics, presented progressive accumulation of clustered, heat shock protein 70–immunopositive neuronal fragments and displayed a high incidence of reactive astrocytes. Our findings suggest that AChE-R serves as a modulator that may play a role in preventing the shift from transient, acute stress to progressive neurological disease.

Both chronic stress and acute stress promote neuroanatomic changes in brains of evolutionarily diverse species, including higher vertebrates and humans (1). Some of these changes likely reflect normal physiological adaptation to injury, environmental challenge, traumatic experience, or even standard maintenance conditions of laboratory animals (2). However, stress may also precipitate delayed or prolonged neuropsychiatric dysfunction, the etiology of which is yet poorly defined. For example, up to 30% of individuals exposed to an acute traumatic experience develop posttraumatic stress disorder, a syndrome characterized by progressively worsening personality disturbances and cognitive impairments (3). The cellular and molecular factors mediating the switch between physiological accommodation of stress and progressive disease are unknown but likely reflect complex interactions between the genetic background of the challenged individual and the nature of the stress insult (3–5). The accepted notion is that physiological stress responses are beneficial in the short run but detrimental if overactivated or prolonged (6). This concept suggests the existence of stress modulators designed to regulate the extent, duration, and long-term impact of acute stress responses.

We recently reported massive induction of a unique mRNA species encoding the rare ''read-through'' variant of acetylcholinesterase (AChE-R) in brains of mice subjected to forced swimming stress (7). AChE-R differs from the dominant ''synaptic'' variant, AChE-S, in the composition of its C-terminal sequence (8). Both enzymes effectively hydrolyze acetylcholine. However, AChE-S can form multimeric complexes and associate with membranes through interactions with structural subunits, whereas AChE-R is monomeric and soluble (9). In hippocampal brain slices, induced AChE-R seemed to play a role in delimiting a state of enhanced neuronal excitation observed after acute cholinergic stimulation (7). This observation suggested that AChE-R acts as a stress modulator in mammalian brain.

Transgenic mice overexpressing human AChE-S in central cholinergic neurons exhibited progressive impairments in learning and memory, diminished dendritic branching, and reduced numbers of spines in cortical neurons (10). Similar behavioral and morphological characteristics were reported in senile dementia (11), a murine model of chronic stress (12), and delayed consequences of anticholinesterase intoxication (7).

The up-regulation of AChE-R under stress, the unique biochemical characteristics of AChE-R compared with AChE-S, and the characteristics of neurodegenerative disease manifested in AChE-S transgenic mice, together raised the question of whether AChE-R is involved in the shift from acute stress response to neurodegenerative state. To study this issue, we compared two lines of transgenic mice overexpressing human AChE-R (13) with AChE-S transgenic and control FVB/N mice. We hypothesized that if AChE-R promotes neurodegeneration, transgenic animals with chronic overexpression of this protein would display neuroanatomical markers of neuronal pathology even when confronted only with the mild stresses of daily life. On the other hand, if AChE-R works against the slide into neurodegeneration, AChE-R transgenics should display markers of neuroprotection. Herein, we report that AChE-R transgenic mice are indeed relatively free of some neuronal stress correlates compared with controls, whereas AChE-S transgenics display accelerated, age-dependent accumulation of neuroanatomical features indicative of neuronal stress responses. This study points at AChE-R as a stress-induced modulator of delayed neural stress response processes that can protect the mammalian brain from neurodegenerative disease, perhaps by preventing AChE-S from causing such deterioration.

Methods

Animals. Mice were killed by cervical dislocation, and tissues were rapidly excised and frozen. Homogenates were prepared in nine volumes of 0.01 M Na-phosphate buffer, pH 7.4/1% Triton X-100 (wt/wt), incubated on ice (1 h), and centrifuged (at 14,000

This paper was submitted directly (Track II) to the PNAS office.

Abbreviations: AChE, acetylcholinesterase; AChE-R, read-through AChE variant; AChE-S, synaptic AChE variant; ARP, AChE read-through peptide; GST, glutathione *S*-transferase; GFAP, glial fibrillary acidic protein; NFT200, neurofilament 200; HSP, heat shock protein; GABA, γ-aminobutyric acid; PCP, phencyclidine.

†Present address: Department of Evolution Systematics and Ecology, Institute of Life Sciences, Hebrew University of Jerusalem, 91904, Israel.

‖To whom reprint requests should be addressed. E-mail: soreq@cc.huji.ac.il.

The publication costs of this article were defrayed in part by page charge payment. This article must therefore be hereby marked "*advertisement*" in accordance with 18 U.S.C. §1734 solely to indicate this fact.

Article published online before print: *Proc. Natl. Acad. Sci. USA*, 10.1073/pnas.140004597. Article and publication date are at www.pnas.org/cgi/doi/10.1073/pnas.140004597

rpm for 45 min in an Eppendorf model 5417R centrifuge); supernatants were then collected.

AChE Activity and Protein Concentration. AChE activity and protein concentration determinations were performed as described (13). Sucrose gradient centrifugation was performed as detailed elsewhere (14), except that 0.5% Triton X-100 was used as detergent.

Immunoblotting. Immunoblot analysis was performed essentially as detailed (15). Immunodetection was performed with pooled goat anti-mouse and anti-human AChE antibodies directed at an N-terminal peptide common to the different variants (N-19 and E-19; Santa Cruz Biotechnology). Signals were quantified with IMAGE-PRO software (Media Cybernetics, Silver Spring, MD).

Preparation of Antibodies Directed at the AChE Read-Through Peptide (ARP). A glutathione *S*-transferase (GST)-ARP (GMQGPAGSGWEEGSGSPPGVTPLFSP) fusion protein was expressed in *Escherichia coli* and purified by affinity chromatography. Female New Zealand rabbits were immunized with 0.3 mg of ARP-GST in Freund's complete adjuvant and reimmunized monthly with 0.2 mg of ARP-GST in Freund's incomplete adjuvant. Specific serum antibodies were detected by ELISA by using immobilized ARP-GST with excess soluble GST. Crude IgG fraction was prepared by $(NH_4)_2SO_4$ precipitation. IgG fractions were incubated repeatedly with immobilized GST or heat-shocked *E. coli* lysate and eluted with 4.5 M $MgCl_2$. Unbound fractions were incubated with ARP-GST beads, eluted, and dialyzed.

Preparation of Brain Sections. Mice were deeply anesthetized with Fluothane (Zenaca, Macclesfield Cheshire, U.K.) and transcardially perfused with 4% (vol/vol) paraformaldehyde. Brains were postfixed in 4% (vol/vol) paraformaldehyde (overnight, 2–8°C) and incubated in 15% (vol/vol) sucrose/0.1 M PBS. Coronal cryostat sections (30 μm) were floated in PBS and kept at −20°C in 40% (vol/vol) ethylene glycol/1% polyvinylpyrrolidone/0.1 M potassium acetate (pH 6.5) until staining.

Immunohistochemistry. Immunohistochemistry was performed as described (16). Staining was with extravidin-peroxidase (Sigma) reacted with diaminobenzidine and nickel ammonium sulfate. Silver impregnation to detect degenerating argyrophilic neurons was performed by using kit PK301 (FD Neurotechnologies, Ellicott City, MD). Antibody dilutions were mouse anti-neurofilament 200 (NFT200; clone N52, Sigma; 1:200); mouse anti-heat shock protein 70 (HSP70; clone BRM22, Sigma; 1:125); mouse anti-glial fibrillary acidic protein (GFAP; clone GA5, Sigma; 1:500); mouse anti-calbindin D28K (clone CL-300, Sigma, 1:500); mouse anti-parvalbumin (clone P19, Sigma 1:500); mouse anti-human erythrocyte AChE (Chemicon; 1:500); and the above described rabbit anti-ARP antiserum (1:100).

Results

AChE-R and AChE-S Are Moderately Overexpressed in Brains of Transgenic Mice. Catalytic activity measurements showed moderately elevated AChE activity in cortex, hippocampus, and basal nuclei of mice from two independent AChE-R transgenic lines (lines 45 and 70; ref. 13) and a single line of AChE-S transgenics (10), as compared with controls (Fig. 1*A*). Immunoblot analysis of cortex homogenates with antibodies directed at the N-terminal domain common to all AChE variants revealed two to three immunoreactive bands, probably reflecting posttranslational processing. The top two bands appeared more intense in transgenics. Cumulative densitometry of all three bands revealed that AChE immunoreactivity was modestly elevated in cortex of both AChE-R and AChE-S transgenics as compared with controls (Fig. 1*B*). In contrast, sucrose gradient centrifugation

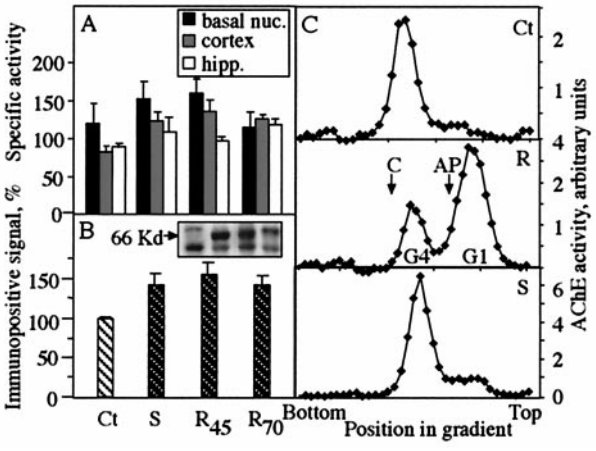

Fig. 1. Overexpression of AChE in transgenic brain. (*A*) AChE activity in brain regions of transgenic mice. Shown are rates of acetylthiocholine hydrolysis per min per mg of protein in homogenates of basal nuclei (basal nuc.), cortex, and hippocampus (hipp.) of AChE-S (S), AChE-R of line 45 (R_{45}), AChE-R of line 70 (R_{70}) transgenics, and control (Ct) mice, all from the FVB/N strain. Bars present averages ± SEM for homogenates from four or five mice of each pedigree. Note that elevation in catalytic AChE activity, although nonsignificant, is common to all transgenic lines. (*B*) AChE immunoreactivity in cortex of transgenic mice. Shown are average intensities ± SEM of immunopositive bands after SDS/PAGE, immunoblot, and densitometric analyses of cortical homogenates from transgenic and control mice. The antibody used was targeted against the common N-terminal domain of AChE; the positive signal obtained with this antibody in control mouse samples (see *Inset*) demonstrates massive cross reactivity with the mouse enzyme. Intensities were determined for the three main immunopositive bands (see *Inset*) from five to eight lanes loaded with protein from individual mice of each strain and are presented as percentage of control values within the same gel. Note that elevation in immunoreactivity, although nonsignificant, is common to all transgenic lines. (*B Inset*) An example of an immunoblot film, showing the main bands in each lane for each of the transgenics and controls at the same order as in the bar graph. Kd, kilodalton. (*C*) Altered multimeric assembly. Shown are sucrose gradient profiles for AChE in the cortex of control (Ct), AChE-S (S), and AChE-R (R; line 45) mice. Arrows denote the sedimentation of bovine catalase (C; 11.4 S) and alkaline phosphatase (AP; 6.1 S). Note elevation in AChE tetramers (G4; ≈10 S) or monomers (G1; ≈4.4 S) and the altered ratio between these isoforms in the different transgenics.

demonstrated a large increase of AChE monomers in the cortex of AChE-R mice (Fig. 1*C*). The ratio between tetramers and monomers was 11.0, 7.4, and 0.4 in cortices of control, AChE-S transgenic, and AChE-R transgenic mice, respectively. That the ratio between tetramers and monomers was altered more substantially than the absolute elevation of enzyme activity in AChE-R mice suggested that the multimeric assembly of AChE in brain depends on the ratio of AChE-S to AChE-R monomers.

Immunological Detection of AChE-R in Mammalian Brain. An antiserum directed at human ARP unique to the AChE-R isoform was used to immunostain frozen coronal brain sections. Anti-ARP antiserum stained neurons, but not glia, from both control and transgenic mice (Fig. 2). In sections from AChE-R transgenic mice, intense neuronal staining, apparent both in soma and dendrites, was noted in somatosensory and piriform cortex, dentate gyrus, and basolateral amygdala (Fig. 2 *Right*), presumably reflecting prominent expression of human AChE-R in these regions. Dendritic staining was limited to proximal regions, except for dentate gyrus neurons, where distal dendritic regions (at least 70 μm in length) were stained as well. Many additional neurons in these brain regions exhibited weak to moderate staining of the cytoplasm, leaving the nucleus completely pale. In addition, prominent staining of some neurons was observed in the hypothalamus, thalamus, and nucleus basalis magnocel-

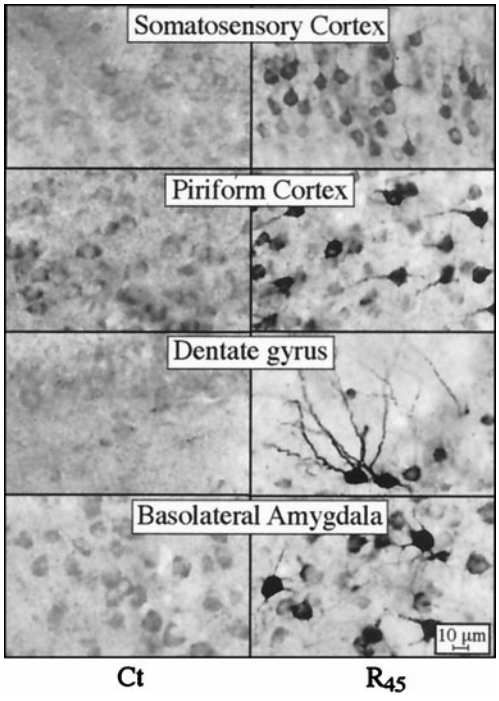

Fig. 2. AChE-R immunoreactivity in transgenic brain. Shown is AChE-R immunoreactivity in high-magnification photomicrographs of coronal sections 1.2 mm posterior to bregma from the brains of control (Ct) mice and the AChE-R line 45 transgenics (R_{45}). Note that ARP immunostaining is apparent only in neurons, that both somata and processes are stained, and that the intensity of neuronal staining is highly variable between the different brain regions.

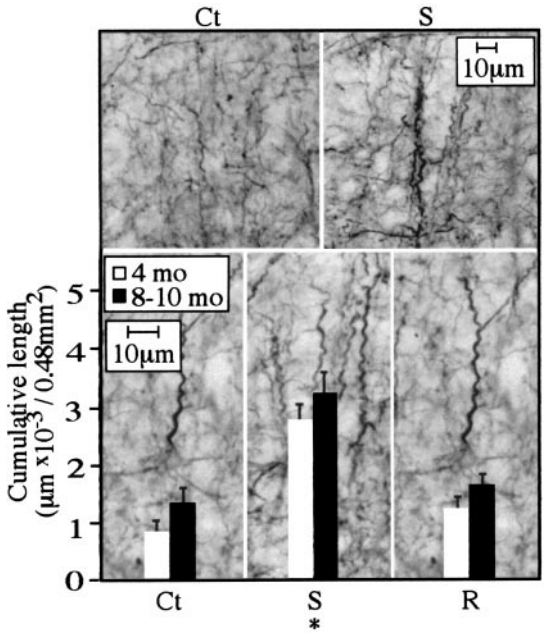

Fig. 3. Evidence for neuronal process malformation in AChE-S transgenic mice. (*Upper*) Example micrographs from control (Ct) and AChE-S transgenics (S) immunolabeled for NFT200. (*Lower*) Cumulative lengths (averages ± SEM) of all axonal or dendritic segments displaying a corkscrew-like pattern are displayed on high-magnification micrographs from the parietal cortex of 4-month-old or 8- to 10-month-old AChE-S (S) and AChE-R (R) transgenics and control (Ct) mice. Numbers were derived from three coronal sections containing the somatosensory cortex, 1–2 mm posterior to bregma, from each of six male mice per group. Analysis with the Seescan Image Analysis system (Seescan plc, Cambridge, U.K.) was performed on 32 subfields of 150 μm (width) × 100 μm (height; total area of 0.48 mm^2). *, $P < 0.001$.

lularis neurons (data not shown). Both staining intensity and numbers of stained neurons were higher in line 45 than in line 70 mice. Weak, diffuse staining was also observed in many brain regions of control and AChE-S transgenic mice (Fig. 2 and data not shown). In control mice, however, somewhat pronounced AChE-R accumulation was noted in piriform cortex and basolateral amygdala. Control sections exposed to antiserum preadsorbed with synthetic ARP (10 μM) were completely negative (data not shown), demonstrating specificity of the staining. With antiserum directed at the common domain of the enzyme, only AChE-S transgenic mice displayed immunopositive signals. In this case, the antibody labeled neurons in the nuclei of the basal ganglia, including striatum, globus pallidus, nucleus basalis magnocellularis, entopeduncular nucleus, and substantia nigra pars reticulata. Overall, the immunodetection of AChE-R and AChE-S in transgenic mice was consistent with *in situ* hybridization data localizing expression of the various mRNAs to the same brain regions (ref. 10 and data not shown). Thus, the failure of anti-common-domain antiserum to stain AChE-R overexpressing neurons may reflect differential folding properties of AChE-S (17) and AChE-R monomers.

Indication for AChE-S-Induced Neuronal Hyperexcitation. Because AChE overexpression in mammalian and amphibian systems affected neuronal processes (10, 15), we compared process morphology in control and AChE transgenic mice. Immunostaining with a monoclonal antibody to the cytoskeletal protein NFT200 revealed a curled ''corkscrew''-like deformation of cortical, but not hippocampal, processes in all mouse lines (Fig. 3). Corkscrew processes, which are indicative of neuronal hyperexcitation (18), exhibited an invariant sinusoid-like regularity and did not stain for HSP70. To quantify the extent of corkscrew formation, we measured the cumulative length of neurites with corkscrew morphology in 500-μm^2 regions. The cumulative length of corkscrew-shaped neurites progressed with age from 4 to 8–10 months, in all pedigrees. However, at both 4 months and 8–10 months of age, AChE-S mice displayed significantly greater extents of corkscrew morphology than either control or AChE-R transgenic mice. In striking contrast, both lines of AChE-R transgenic mice displayed a degree of corkscrew morphology comparable with that of control mice (Fig. 3 and Table 1). Because deterioration of cortical inhibitory GABAergic interneurons was suggested to be the cause of the corkscrew phenomenon (18), we characterized GABAergic neurons in the somatosensory cortex of transgenic mice. No cell loss or shrinkage and no morphological aberrations were observed among any of the transgenic pedigrees as compared with controls (Table 1). Moreover, average thickness of the parietal cortex and neuronal density were similar between the different lines. Furthermore, silver impregnation did not stain parietal cortex neurons in any of these pedigrees, showing no evidence for terminal neurodegeneration (not shown).

AChE-R Protects Hippocampal Neurons from Stress-Related Morphologies. In all pedigrees, some clusters of NFT200-immunoreactive neuronal fragments were observed in the stratum radiatum layer of the hippocampal CA1–3 regions (Fig. 4 *Top*), increasing in number with advancing age (Fig. 4 and Table 1). AChE-S transgenic mice exhibited a significant extent of cluster formation already at 4 months of age, which was approximately doubled in 8- to 10-month-old mice. In contrast, only about one-third of 4-month-old control FVB/N and AChE-R mice exhibited clustered neural fragments, and then, not more than one cluster per mouse was observed. The 8- to 10-month-old

Table 1. Suppressed stress-associated morphological features in AChE-R transgenics

Morphological Abnormality	Measurement	AChE-S	AChE-R	Control	Statistical test
Curled processes, (NFT200)	Cumulative length in 0.48 mm^2 (μm)	3,080 ± 210; $P < 0.0001$	1,410 ± 150	1,070 ± 170	Newman–Keuls
Cortex thickness μm		230 ± 7	240 ± 8	230 ± 5	*F* test
GABAergic interneurons (parvalbumin)	Cell number in cortical layers 1–3	210 ± 4	190 ± 14	190 ± 19	*F* test
	Cell number in cortical layers 4–6	250 ± 12	270 ± 14	250 ± 10	*F* test
	Cell area, μm^2	68 ± 3	66 ± 3	60 ± 3	*F* test
GABAergic interneurons (calbindin D28K)	Cell number in cortical layers 1–3	290 ± 10	300 ± 6	260 ± 15	*F* test
	Cell number in cortical layers 4–6	67 ± 5	73 ± 2	76 ± 5	*F* test
	Cell area, μm^2	57 ± 2	55 ± 1.5	54 ± 2	*F* test
Neuronal fragment clusters (NFT200)	Number of clusters per section	3.3 ± 0.8	0.4 ± 0.2; $P < 0.02$	1.7 ± 0.4	Mann–Whitney
	Cluster area, μm^2	3,470 ± 370	2,090 ± 500*	2,060 ± 230	*T* test
	Number of fragments per cluster	110 ± 16; $P < 0.002$	70 ± 15*	46 ± 4	*T* test
	Fragment density in cluster	0.032 ± 0.002; $P < 0.03$	0.035 ± 0.008*	0.023 ± 0.002	*T* test
Neuronal fragment clusters (HSP70)	Number of clusters per section	6.2 ± 2.1; $P < 0.005$	0.4 ± 0.3	1.7 ± 0.7	Mann–Whitney
	Cluster area, μm^2	2,690 ± 380; $P < 0.03$	1,370 ± 280*	1,690 ± 240	*T* test
	Number of fragments per cluster	50 ± 6; $P < 0.02$	30 ± 7*	31 ± 4	*T* test
	Fragment density in cluster	0.020 ± 0.001	0.022 ± 0.004*	0.019 ± 0.001	*T* test
Astrocytes (GFAP)	Total number of cells	270 ± 9	250 ± 10	270 ± 10	*F* test
	Percentage of hypertrophic cells	24 ± 2	16 ± 3; $P < 0.03$	24 ± 2	Newman–Keuls

Presented are average values ± SEM for the measurements of morphological features noted in the text. The antibody used for staining is noted in parentheses. Age groups of 4-month-old and 8- to 10-month-old mice were combined for calculations, except for the clustering phenomenon, which increased with age, and for which, the data presented (pooled from three mice) is for the 8- to 10-month-old group. A normal distribution could not be assumed, and nonparametric tests were used: Kruskal–Wallis's for the main effects of transgenic line or age and Mann–Whitney's for multiple comparisons of transgenic lines. Significant *P* values (in comparison with control mice) are noted where appropriate. GABA; γ-aminobutyric acid.

*In AChE-R transgenics, the small number of clusters found precluded any statistical comparison of cluster area and number of fragments per cluster.

control mice displayed approximately half the number of fragment clusters as age-matched AChE-S mice. In 10-month-old AChE-R mice, clustered neuronal fragments were very rare. Cluster size, the number of fragments per cluster, and fragment density were all significantly greater in 8- to 10-month-old AChE-S mice than in age-matched controls or AChE-R transgenics (Table 1).

Neuronal fragment clusters have been observed in posttraumatic states, for example after head injury (19–21). Therefore, we stained sections for HSP70, which stains degenerating processes in acute head trauma (19, 20) and Alzheimer's disease (22). Anti-HSP70 antibodies revealed clusters in hippocampus resembling those observed with anti-NFT200, with similar patterns and incidence (Fig. 4 and Table 1). As with NFT200-stained clusters, HSP70-positive clusters were more abundant in AChE-S and more sparse in AChE-R mice than in controls. Progression with age, from 4 to 8 months, was observed both in control and AChE-S mice ($P = 0.05$) but not AChE-R mice. In no case were hippocampal neurons stained by silver impregnation, demonstrating sustained cell viability.

Suppressed Astrocyte Reactivity in AChE-R Transgenic Mice. Immunostaining for GFAP was performed to test whether the neuroanatomic changes in cortical and hippocampal neurons overexpressing the different AChE variants involve morphological changes in glial cells. Modified astrocyte morphology was observed in the stratum lacunosum moleculare of the hippocampal CA3 subregion, where a subset of reactive astrocytes presented highly immunoreactive soma and enhanced dendritic staining (Fig. 5) as compared with normal astrocytes in which the soma were pale or invisible. Only minor differences were discerned in the average total numbers of astrocytes. However, the percentage of reactive astrocytes was significantly lower in the AChE-R transgenics than in controls or AChE-S transgenics (Table 1 and Fig. 5).

Discussion

After acute stress, the ratio between AChE-R and AChE-S increases dramatically, probably by a combination of transcriptional and posttranscriptional mechanisms (7). To test whether prolonged modulation of AChE expression could influence neuroanatomic features in the mammalian brain, we generated transgenic mice with subtle overexpression of either AChE-S or AChE-R in brain neurons. The 30–50% elevated expression of AChE in these transgenic models resembles that observed by us for FVB/N mice subjected to forced swim stress. We therefore hypothesized that if excess AChE-R exacerbates the cumulative neurological consequences of stress, AChE-R transgenics would display exaggerated histopathological features characteristic of stress response processes. In fact, we observed reduced numbers and sizes of clustered neuronal fragments and decreased numbers of reactive astrocytes in 8- to 10-month-old AChE-R transgenic mice compared with controls. Therefore, our data indicate that AChE-R works to protect the brain against neurodegeneration. The inverse pattern of morphological correlates in AChE-S transgenic mice points to AChE-S as a potential accelerator of stress-promoted neurodeterioration.

The predominance of 3′ unspliced AChE-R mRNA in brain after stress represents a diversion of alternative splicing that was also observed in stress responses for the retinal *N*-methyl-D-aspartate receptor I, clathrin light chain B, and transformer-2 β (23). Similarly, stress hormone-induced shifts in alternative splicing were reported to favor the repetitive firing variants of K^+ channels in adrenal chromafin tissue (24). The primary differences between AChE isoforms are reflected in the enzyme's oligomeric assembly, hydrodynamic properties, and subcellular distribution (9). These features will affect the sites of potential action of the enzyme, both with respect to catalytic and noncatalytic activities. That AChE-S, but not AChE-R, accelerates the corkscrew phenomenon attributes a previously unperceived role in neurite degeneration to this AChE variant. Several observations support the notion that AChE-S activates a unique

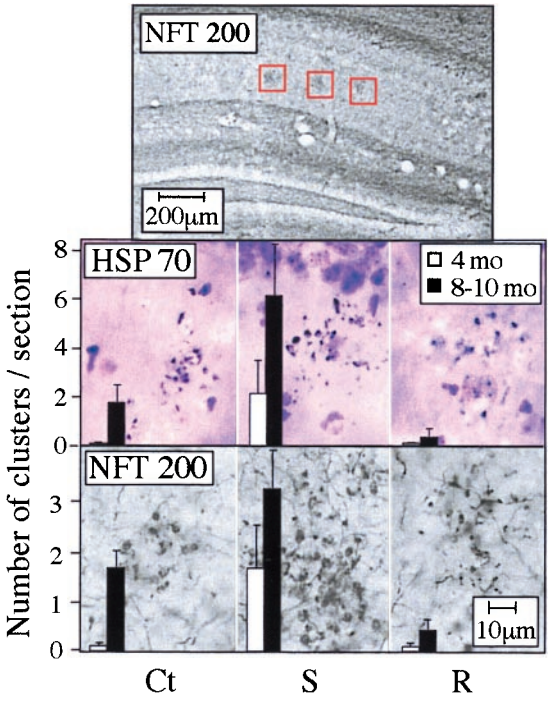

Fig. 4. Clustered neuronal fragments. Shown are coronal brain sections from 8- to 10-month-old control and transgenic mice after immunostaining of NFT200 or HSP70 with cresyl violet counter staining. (*Top*) Low-magnification image, in which gray-black clusters of neuronal fragments immunopositive for NFT200 (surrounded by red frames) are apparent in the stratum radiatum layer of hippocampal CA1–3 regions (1.6–2.8 mm posterior to bregma). (*Middle and Bottom*) High-magnification images of the framed regions, stained for HSP70 and NFT200, respectively. Clusters including over 10 neuronal fragments were counted in three sections from each mouse, 2 to 4 mm posterior to bregma. Bars present counted clusters per section as average ± SEM for six mice from each strain and age group (4-month-old and 8- to 10-month-old). Ct, control FVB/N mouse; S, AChE-S transgenic mouse; R, AChE-R transgenic mouse.

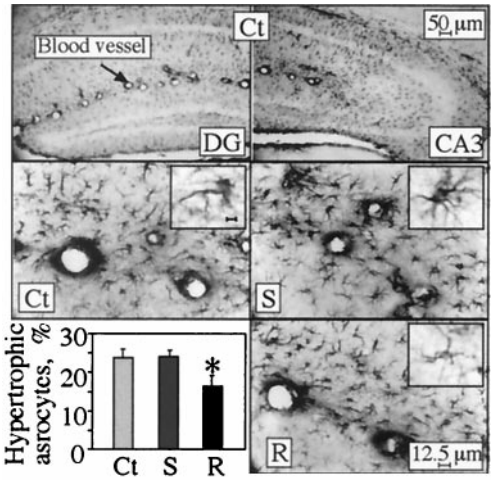

Fig. 5. Astrocyte reactivity. Normal and reactive astrocytes were counted in the stratum lacunosum moleculare in hippocampal sections 2 to 4 mm posterior to bregma (three from each of six mice in each strain). Shown is GFAP astrocyte labeling in coronal brain sections from 4-month-old transgenic and control mice. Note that in normal astrocytes, only dendrites are stained, and soma are pale or invisible, whereas reactive cells display highly immunoreactive soma and enhanced dendritic staining. (*Top*) Example low-magnification micrographs of dentate gyrus (DG; *Left*) and CA3 (*Right*) hippocampal regions of control (Ct) mice. (*Middle and Bottom*) High-magnification images of stratum lacunosum moleculare from the hippocampal CA3 subregion from control (Ct), AChE-S (S), and AChE-R (R) mice. (*Insets*) Individual astrocytes stained for GFAP (Bar = 1 μm). (*Bottom Left*) Percentage of reactive astrocytes of the total counted astrocytes (average ± SEM of $n = 6$ mice for each group). *, $P < 0.05$.

cell-signaling cascade or cascades. For example, in the embryonic spinal cord, AChE-S overexpression was shown to enhance the production of choline acetyl transferase (25). The difference between AChE-S and AChE-R transgenics in this respect probably includes a component related to noncatalytic properties of the two variants. Interestingly, increased ratios between AChE monomers and tetramers, perhaps reflecting AChE-R overproduction, were reported for Alzheimer's disease (26) and after anticholinesterase exposure (reviewed in ref. 27).

We previously reported that chronic overexpression of AChE-S causes progressively impaired memory and decreased dendritic branching in cortical neurons (10), as in senile dementia (11). Our current work demonstrates that AChE-S transgenics manifest additional features of neuronal stress, such as corkscrew processes, neuronal retraction balls, and reactive gliosis. NFT200-positive structures are subject to morphological changes in both the normal and the pathological ranges of plasticity (19, 20, 28). Sinusoidal corkscrew processes were shown after chemical [e.g., phencyclidine (PCP); "angel dust"] intoxication, head trauma, and ischemic/hypoxic stress and in brains of patients with Alzheimer's disease (19–21, 29). This deformity often precedes process degeneration and neuronal death but may also be reversible. The pathway that creates the corkscrew phenotype is considered to be associated with hyperexcitation. For example, PCP, an antagonist of *N*-methyl-D-aspartate receptors on inhibitory GABAergic interneurons, causes hyperactivation of cortical pyramidal neurons with which these interneurons communicate (18). Because muscarinic receptor blockers prevent formation of PCP-induced corkscrew structures (21), this hyperactivation is apparently caused by the excitatory inputs to cortical pyramidal neurons, which include a cholinergic element.

AChE-R transgenics displayed relatively prominent overexpression of the AChE-R protein in precisely those neurons that are notably associated with stress responses in the dentate gyrus, amygdala (30), and piriform cortex (31). Corkscrew structures were increased significantly in AChE-S but not in AChE-R transgenics as compared with control mice, supporting the notion of a protective role for AChE-R. Based on the PCP model, we expected to find pathology among GABAergic neurons and/or increased cholinergic input in AChE-S mice. Because we found no evidence of pathology to GABAergic neurons, there remains the possibility of excessive cholinergic input. Elevated high-affinity choline transport in these mice (10) and elevated acetylcholine levels as measured by microdialysis (C. Erb, unpublished work) indeed indicate cholinergic hyperexcitation.

Clustered neuronal fragments reflecting axonal and dendritic "retraction balls," depict advanced neurite changes (19–21). Elevated HSP70 reported after head injury and in Alzheimer's disease (19, 22) highlights the importance of these clustered neural fragments as markers of neurodeterioration. Although these fragments often predict subsequent neuronal death (20), silver impregnation excluded exceptional rates of neuronal death among AChE-S transgenics, both in the parietal cortex where corkscrew-like processes appeared and in the hippocampus where the process retraction balls were seen. Cluster numbers and sizes and fragment numbers and density within clusters were significantly elevated in 8- to 10-month-old versus 4-month-old control mice and in AChE-S transgenics versus controls in both ages. Thus, AChE-S seemed to accelerate a normal age-

dependent neuropathological process. In contrast, AChE-R prominently attenuated cluster formation in both age categories. The possibility that the protective effects of AChE-R derive from a direct interaction or competition with AChE-S or its putative cell surface ligands remains to be studied. One way to approach this question would be to establish transgenic mice overexpressing both transcripts. In cultured glioma cells coexpressing AChE-S and AChE–R mRNAs, AChE-R exerted a dominant phenotype (32).

GFAP overproduction in astrocytes is considered to reflect neuronal changes such as synaptic remodeling (33). Reactive astrocytes, significantly reduced in the hippocampus of AChE-R transgenics as compared with controls or AChE-S transgenic mice, are the hallmark of "reactive gliosis," reflecting the reaction of glial cells to trauma. Reactive gliosis occurs in acute brain injury, in neurodegenerating regions within the brain of patients with Alzheimer's, during viral infections, after chemical intoxication (34), and even in normal aging (35). The low incidence of reactive glia in AChE-R transgenic mice further reinforces the notion that chronic presence of AChE-R acts to protect the brain against long-term stress-related damage.

In this study, mice were not subjected to experimental stress but were exposed to mildly stressful daily handling (2). However, they developed features associated with stress in numerous species and various stress paradigms (18–22, 29, 33–37). However, genetic background may have a significant effect on the rate and extent of stress-induced neurodeterioration. Different strains of mice may vary in fearfulness and response to stress (38). FVB/N mice were shown to be highly susceptible to the widespread neurodegeneration that follows kainic acid seizures (39) but not to the selective loss of midbrain dopaminergic neurons induced by 1-methyl-4-phenyl-1,2,3,6-tetrahydropyridine (40) as compared with the C57BL/6 mice. No evidence for neuronal loss was found in AChE-S transgenic mice with the FVB/N background up to 10 months of age. Nevertheless, these animals can live up to 2 years, and neuronal death may occur only at truly advanced ages.

Chronic overexpression of AChE-R was consistently associated with reduction in several morphological correlates of neurodegeneration in transgenic mice. Demonstration of such association in two distinct transgenic lines shows that this phenotype did not depend on the integration site of the transgene but probably on a certain threshold of AChE-R overexpression. Our current findings therefore demonstrate that AChE-R, most likely with another modulator or modulators, may be beneficial in the response to acute stress at two levels: (*i*) by dampening the acute cholinergic hyperactivation that accompanies stress (7) and (*ii*) by protecting the brain from entering the downward spiral into progressive neurodegeneration through an as-yet unidentified mechanism, which could involve noncatalytic activities and/or direct competition with AChE-S. In that case, the diversion of up-regulated AChE expression after insults to the central nervous system from production of the usual AChE-S to the unusual AChE-R isoform (7) would reflect an elegant evolutionary mechanism to avoid the dangers of overexpressed AChE-S. These findings imply that mutations conferring heritable up-regulation of AChE-R would protect the mammalian central nervous system from some age-dependent neuropathologies. The definitive role of AChE-R after transient stress or drug-induced overexpression remains to be examined in additional animal models permitting conditional regulation of AChE gene expression.

We thank Dr. S. Seidman (Jerusalem) for critically reviewing this manuscript. This study was supported by U.S.–Israel Binational Science Foundation Grant 96-00110 to H.S. and J.W.P. and by grants to H.S. from the Israel Science Fund (number 590/97), Ester Neurosciences, the U.S. Army Medical Research and Materiel Command (DAMD 17-99-1-9547), and the research fund in memory of Leopold, Sara, and Norman Israel. C.F.-F. was the incumbent of a FEBS Long-Term Fellowship.

1. McEwen, B. S. (1999) *Annu. Rev. Neurosci.* **22,** 105–122.
2. Riley, V. (1981) *Science* **212,** 1100–1109.
3. Turnbull, G. J. (1998) *Injury* **29,** 169–175.
4. True, W. R., Rice, J., Eisen, S. A., Heath, A. C., Goldberg, J., Lyons, M. J. & Nowak, J. (1993) *Arch. Gen. Psychiatry* **50,** 257–264.
5. Graham, D. I., Gentleman, S. M., Nicoll, J. A., Royston, M. C., McKenzie, J. E., Roberts, G. W., Mrak, R. E. & Griffin, W. S. (1999) *Cell. Mol. Neurobiol.* **19,** 19–30.
6. Sapolsky, R. M. (1996) *Science* **273,** 749–750.
7. Kaufer, D., Friedman, A., Seidman, S. & Soreq, H. (1998) *Nature (London)* **393,** 373–377.
8. Grisaru, D., Sternfeld, M., Eldor, A., Glick, D. & Soreq, H. (1999) *Eur. J. Biochem.* **264,** 672–686.
9. Seidman, S., Sternfeld, M., Ben Aziz-Aloya, R., Timberg, R., Kaufer-Nachum, D. & Soreq, H. (1995) *Mol. Cell. Biol.* **15,** 2993–3002.
10. Beeri, R., Le Novere, N., Mervis, R., Huberman, T., Grauer, E., Changeux, J. P. & Soreq, H. (1997) *J. Neurochem.* **69,** 2441–2451.
11. Buell, S. J. & Coleman, P. D. (1981) *Brain Res.* **214,** 23–41.
12. Sakic, B., Szechtman, H., Denburg, J. A., Gorny, G., Kolb, B. & Whishaw, I. Q. (1998) *J. Neuroimmunol.* **87,** 162–170.
13. Sternfeld, M., Patrick, J. D. & Soreq, H. (1998) *J. Physiol. (Paris)* **92,** 249–255.
14. Flores-Flores, C., Martinez-Martinez, A., Munoz-Delgado, E. & Vidal, C. J. (1996) *Biochem Biophys. Res. Commun.* **219,** 53–58.
15. Sternfeld, M., Ming, G., Song, H., Sela, K., Timberg, R., Poo, M. & Soreq, H. (1998) *J. Neurosci.* **18,** 1240–1249.
16. Shoham, S. & Ebstein, R. P. (1997) *Exp. Neurol.* **147,** 361–376.
17. Bourne, Y., Grassi, J., Bougis, P. E. & Marchot, P. (1999) *J. Biol. Chem.* **274,** 30370–30376.
18. Olney, J. W. & Farber, N. B. (1995) *Arch. Gen. Psychiatry* **52,** 998–1007.
19. Li, R., Fujitani, N., Jia, J. T. & Kimura, H. (1998) *Am. J. Forensic Med. Pathol.* **19,** 129–136.
20. Kubo, S., Kitamura, O., Orihara, Y., Ogata, M., Tokunaga, I. & Nakasono, I. (1998) *J. Med. Invest.* **44,** 109–119.
21. Corso, T. D., Sesma, M. A., Tenkova, T. I., Der, T. C., Wozniak, D. F., Farber, N. B. & Olney, J. W. (1997) *Brain Res.* **752,** 1–14.
22. Hamos, J. E., Oblas, B., Pulaski-Salo, D., Welch, W. J., Bole, D. G. & Drachman, D. A. (1991) *Neurology* **41,** 345–350.
23. Daoud, R., Da Penha Berzaghi, M., Siedler, F., Hubener, M. & Stamm, S. (1999) *Eur. J. Neurosci.* **11,** 788–802.
24. Xie, J. & McCobb, D. P. (1998) *Science* **280,** 443–446.
25. Andres, C., Beeri, R., Friedman, A., Lev-Lehman, E., Henis, S., Timberg, R., Shani, M. & Soreq, H. (1997) *Proc. Natl. Acad. Sci. USA* **94,** 8173–8178.
26. Saez-Valero, J., Sberna, G., McLean, C. A. & Small, D. H. (1999) *J. Neurochem.* **72,** 1600–1608.
27. Kaufer, D., Friedman, A. & Soreq, H. (1999) *The Neuroscientist* **5,** 173–183.
28. Trojanowski, J. Q., Walkenstein, N. & Lee, V. M. (1986) *J. Neurosci.* **6,** 650–660.
29. Braak, E., Braak, H. & Mandelkow, E. M. (1994) *Acta Neuropathol.* **87,** 554–567.
30. Herman, J. P. & Cullinan, W. E. (1997) *Trends Neurosci.* **20,** 78–84.
31. Imaki, T., Shibasaki, T., Hotta, M. & Demura, H. (1993) *Brain Res.* **616,** 114–125.
32. Karpel, R., Sternfeld, M., Ginzberg, D., Guhl, E., Graessmann, A. & Soreq, H. (1996) *J. Neurochem.* **66,** 114–123.
33. Laping, N. J., Teter, B., Nichols, N. R., Rozovsky, I. & Finch, C. E. (1994) *Brain Pathol.* **4,** 259–275.
34. Wu, V. W. & Schwartz, J. P. (1998) *J Neurosci. Res.* **51,** 675–681.
35. Unger, J. W. (1998) *Microsc. Res. Tech.* **43,** 24–28.
36. Faden, A. I. (1993) *Crit. Rev. Neurobiol.* **7,** 175–186.
37. Ma, K. C., Nie, X. J., Hoog, A., Olsson, Y. & Zhang, W. W. (1994) *J. Neurol. Sci.* **126,** 184–192.
38. Francis, D. D. & Meaney, M. J. (1999) *Curr. Opin. Neurobiol.* **9,** 128–134.
39. Schauwecker, P. E. & Steward, O. (1997) *Proc. Natl. Acad. Sci. USA* **94,** 4103–4108.
40. German, D. C., Nelson, E. L., Liang, C. L., Speciale, S. G., Sinton, C. M. & Sonsalla, P. K. (1996) *Neurodegeneration* **5,** 299–312.